# A novel optimization algorithm based PID controller design for real-time optimization of cutting depth and surface roughness in finish hard turning processes

Abdul Muqeet [a], Asif Israr [a], Muhammad Hamza Zafar [b], Majad Mansoor [c], Naureen Akhtar [b,*]

[a] *Department of Mechanical Engineering, Institute of Space Technology, Islamabad, 44000, Pakistan*
[b] *Department of Engineering Sciences, University of Agder, Grimstad, 4879, Norway*
[c] *Department of Automation, University of Science and Technology of China, Hefei, 270003, China*

## ARTICLE INFO

## ABSTRACT

This paper proposes a novel method to improve surface finish in turning processes by effectively controlling the cutting depth. A metaheuristic algorithm based PID control system, in combination with a piezoelectric vibration sensor for feedback, is introduced to regulate the position of the servo motor that controls the cutting tool. The PID controller is optimized using Q-learning based Sand Cat Optimization algorithm to achieve the best performance in terms of cutting depth accuracy and surface finish quality. The piezoelectric sensor provides real-time feedback information about the cutting process and allows for precise adjustments to the cutting depth. The results demonstrate the proposed system's ability to handle variations in cutting conditions and tool's wear and tear. Compared to highly optimized standard PID control, improved robustness and stability has been achieved in experimental results by proposed framework. Experimental results demonstrate improved robustness and stability compared to standard PID control. Several materials with high hardness of 20–65 HRC including Phenolic Bakelite, Copper, Thermoplastic, and Stainless Steel (AISI-420, AA6061-T6, and AISI-316) are tested. Minimum value of Vibration amplitude achieved is 0.598 μm for cutting depth of 0.25 mm. The sustained minimum amplitude of vibration and $R_a$ value of the surface finish is found comparable to standard models with less than 10% error.

## 1. Introduction

Machining is crucial in parts manufacturing as it removes material to achieve the desired shape, size, and surface finish. It's widely used in industries such as aerospace, automotive, medical, and manufacturing. Machining aims to produce accurate, consistent, and repeatable parts that meet design specifications while ensuring high quality, reliability, and functionality. Additionally, machining processes must be efficient, cost-effective, and safe for both the operator and the environment. A simple method for tool replacement timing based on tool wear progress, determined through cutting experiments with a high-speed steel end mill. A linear relationship between cutting edge/workpiece contact length and flank wear width was found, and tool replacement timing is determined using correlations between the two. Cutting experiments verified the proposed method's validity [1]. Method for determining the translational quasi-static stiffness of a machine tool is by using the

Stiffness Workspace System (SWS). A methodology for generalized translational static stiffness determination is presented and a case study is conducted on a 5-axis machining center. The importance of analyzing static stiffness distribution is emphasized [2]. An industrial-friendly method for estimating the in-process structural dynamics of machine tools is by using cross Frequency Response Function (FRF) and receptance coupling theory. The proposed method can predict stability diagrams for different tooling systems and estimate cutting forces without requiring costly setup or destructive chatter tests [3] (see Tables 1–3, Fig. 5).

In recent years, significant innovation has been made by gauging parameters through automation of the machining process, optimizing tool geometry, material properties, mathematical optimization of machining parameters, enhancing coolant quantity and most important optimizing vibrations during machining. Turning process is involved in most components manufacturing especially in aerospace industry,

**Table 1**

Parameters of QSCSO algorithm for solving optimization problem.

| Parameter | Value |
|---|---|
| Number particles | 30 |
| Iteration number | 100 |
| $[S_M; \theta;]$ | $[2; 0-360;]$ |
| Lower bound of $[K_p; K_i; K_d]$ | $[0.001; 0.001; 0.001]$ |
| Upper bound of $[K_p; K_i; K_d]$ | $[20; 20; 20]$ |
| Dimension for optimization problem | 3 |
| Simulation time, $t_{sim}$ | 1s |

**Table 2**

Physical properties of AISI420 [4].

| Condition | Tensile Strength, MPa | Yield Strength, MPa | Hardness, HRC | Density, kg/m$^3$ |
|---|---|---|---|---|
| Annealed | 600 | 310 | 25–30 | 7800 |
| Hardened | 1550 | 1300 | 50–55 | – |

**Table 3**

Chemical properties of AISI420 [4].

| C | Cr | Ni | Si | Al | S |
|---|---|---|---|---|---|
| 0.36 | 13.87 | 0.19 | 0.28 | 0.005 | 0.018 |
| **Mo** | **Mn** | **Sn** | **Cu** | **P** | **Fe** |
| 0.04 | 0.52 | 0.005 | 0.04 | 0.019 | Rest |

automobile, product line and agriculture. Turning tools and subject has been used since centuries and most recently provided the base for modern automated manufacturing processes. Surface finished influenced by smartly optimizing CUTTING SPEED, cutting feed, cutting depth demonstrated are elaborated in-depth in Refs. [5–7]. Several classes of parameters optimization techniques such as particle swarm method [8], Taguchi optimization method [9,10], Genetic algorithm [11], and Artificial neural network [12] are well deliberated conforming to the machining objective requirements. In view of modified turning processes self-adaptive system "*Auto-resonant Ultrasonic-vibration Cutting unit*" [13] enhanced dynamic properties of tuning. Dynamic response of cutting tool during turning process value-added up to 77% using "*Electro Magneto Rheological Damper*" [14]. "*Low Frequency Vibration Cutting*" has been performed by formulating chip breaking conditions that enabled difficult to turn materials in Ref. [15], whereas investigation in Refs. [16,17] compared the reduction in cutting force during linear and elliptical "*vibration assisted micro groove turning*" mechanism. Different materials behave differently during turning process and catered systematically such as AISI420 using cryogenic cooling and MQL environment in Refs. [4,18], turning of AISI316 investigated and optimized in Refs. [19,20]. Tool wear was characterized during finish turning of AISI1045 in Refs. [21,22]. The effect of parameters during turning of AA6061-T6 on surface roughness and material removal rate using response surface methodology is illustrated in Ref. [23]. In the same way parametric response for pure copper [24], aluminum bronze [25], phenolic Bakelite [26], and thermoplastic [27] has been optimized either analytically or experimentally [28].

Vibration assisted machining being the evolving technique has gained much importance. Modal analysis, optimization algorithm, effect of tool wear and surface roughness, vibrations monitoring, analytical techniques and enormous experimentation with expensive equipment and setup is obligatory. Extensive research is made in this regard to augment turning process parameters [29–33].

Studies proposes a method to mitigate torsional oscillations in polycrystalline diamond compact (PDC) bits during deep drilling. The study investigates the rate effect of cutting forces using a modified bonded-particle model for rock and identifies influencing factors on rate dependency. The results provide insights for improving cutter design

against undesirable rate effects [34]. While a distributed parameter method to model the machining stability of thin-wall components, accounting for regenerative effects in both radial and axial directions. The method constructs 3-D stability lobe diagrams in terms of width/depth of cut, rotational speed, and cutting position. The approach offers a means to identify parameters of a coupled WP-CT system and predict the spatially distributed vibrations and their effects on machining stability. The model was analyzed in simulation and validated with experiments [35].

The miniaturization of consumer products has led to increased micro-milling operations, but cutting-tool wear can impact part quality and production costs. An adaptive control optimization system is proposed to estimate wear and adapt cutting conditions, reducing production costs by up to 29%. Particle swarm optimization performs best [36]. In CNC systems, machining variables are determined by the part programmer, based on experience and knowledge. Adaptive control aims to improve production rate and part quality by calculating and setting optimal variables during machining based on real-time measurements, and subsequent adjustment subject to constraints to optimize performance [37]. An intelligent adaptive control system proposed for finish turning of hardened AISI D2 with optimization methodology to optimize material removal rate and machining cost while maintaining surface quality. The helical gear reverse engineering using evolutionary optimization is achieved by Ref. [38] in short time and higher finishing considering several critical parameters. The system uses wavelet packet transform to estimate tool wear and artificial intelligence techniques for modeling and optimization. The proposed system is found to be 25.6% more efficient than traditional CNC turning systems [39].

The injection molding process is evaluated for internal and external defects. The Taguchi method is used to determine the best levels of geometric and injection machine inputs. The study focuses on developing an accurate model with low computational load using the genetic programming method to calculate the optimal parameters of the process. The results show lower mean square errors compared to previous methods [40]. The importance of reverse engineering in designing complex spare parts in the manufacturing and automobile industries. The paper proposes a methodology for reverse-engineering gears using measurement over balls and span measurement, along with evolutionary optimization techniques. Advanced optimization techniques such as Grey Wolf Optimization, Whale Optimization, Particle Swarm Optimization, and Genetic Algorithm are compared, and confirmatory experiments reveal the effectiveness and accuracy of Grey Wolf Optimization and Particle Swarm Optimization techniques [38]. A hybrid approach, PSO-RDNN, for multi-performance optimization of machining parameters in finish turning of hardened AISI D2. Similarly, optimized injection problem was solved using Genetic programming and interior point solver for thin-walled polypropylene part in Ref. [41]. RPM and feed rate are optimized for minimizing operation cost, maximizing tool life, and producing parts with acceptable surface roughness. Neural network models were developed for predicting tool flank wear and surface roughness during the machining process, and optimum cutting parameters were obtained using the trained neural networks and structured hybrid algorithm. The proposed methodology returns a Pareto optimality graph representing optimized cutting variables for various cutting conditions [28].

### 1.1. Paper contribution and organization

In the turning process, achieving both dimensional accuracy and surface finish while maintaining low process cost and avoiding damage to the tool or workpiece are crucial goals.

- In this research, an Arduino-based machining setup is developed to investigate the impact of cutting depth on workpiece surface finish.
- The system is analytically analyzed, and an experimental setup is designed to determine the optimal tool length and cutting depth.

- An Arduino-based intelligent system is then employed to investigate system parameters and reduce unwanted vibration during machining.
- The results are promising, demonstrating excellent surface finish during the turning process.
- The novelty of this article lies in the proposed method of using a metaheuristic algorithm-based PID control system in combination with a piezoelectric vibration sensor for feedback to effectively control cutting depth and improve surface finish in turning processes.
- The optimization of the PID controller using the Q-learning-based Sand Cat Optimization algorithm and the real-time feedback provided by the piezoelectric sensor allows for precise adjustments to the cutting depth and better handling of variations in cutting conditions and tool wear.
- The proposed system demonstrates improved robustness and stability compared to traditional PID control methods, leading to improved machining performance and reduced machining errors.
- The experimental setup was tested on a variety of materials and achieved lower Integral of Time-weighted absolute error (ITEA) and comparable surface finish quality with less than 10% error.

We conducted a comprehensive literature review in Section 2, which provided an overview of the existing research on subject topic. In Section 3, we presented our proposed technique and provided a detailed description of the optimization algorithm. In Section 4, we described the pre-experimental procedures and preparations undertaken prior to conducting the experiments. The experimental methodology and results are presented in Section 5. Finally, in Section 6, we discussed the promising results of our study and provided recommendations for future research in the field of manufacturing.

## 2. Proposed technique

The proposed model is a hybrid framework. Reinforcement learning (RL) and swarm intelligence techniques have been increasingly used in optimizing complex manufacturing processes. In this study, we propose a new approach for machine tooling turning processes that utilizes RL and Sand Cat Swarm Optimization (SCSO) intelligence algorithms to enhance the tuning of the Proportional-Integral-Derivative (PID) controller. The proposed approach employs a reinforcement learning agent to learn the optimal control actions in real-time, while the CAT swarm intelligence algorithm optimizes the hyperparameters of the RL agent. The RL agent receives feedback from the process to improve its control rule iteratively. The accuracy and convergence speed are at key objectives of the mathematical models combining RL and swarm intelligence for advanced manufacturing optimization.

### 2.1. Sand Cat Swarm Optimization (SCSO)

Sand Cat Swarm Optimization (SCSO) is a metaheuristic algorithm that draws inspiration from the behavior of sand cats in their natural habitat [42]. The SCSO algorithm was developed based on the unique characteristics of sand cats, which enable them to thrive in harsh desert environments. These adaptations include having fur on their paws and soles to protect them from extreme temperatures, as well as the ability to detect low-frequency noises and hunt at night. By emulating these traits, the SCSO algorithm aims to improve problem-solving capabilities in complex and challenging environments.

The hunting behavior of sand cats inspired the design of the Sand Cat Swarm Optimization (SCSO) algorithm. This algorithm has the ability to locate a near-optimal solution quickly, similar to how sand cats are able to locate their prey. The SCSO algorithm starts with initializing a population of search agents within a defined search space [42]. To optimize solutions, a fitness function is defined to evaluate each iteration of the algorithm and guide the search towards the desired objective, whether it

is minimization or maximization. The algorithm continues to iterate until a maximum result is achieved based on the fitness function. It is worth noting that every metaheuristic algorithm employs its unique mechanism for reaching the optimal solution.

The SCSO algorithm is a metaheuristic technique that takes inspiration from the actions of sand cats. The search agents in the SCSO algorithm are initialized and utilize their sensitivity, which starts at 2 kHz, to explore for a solution that is close to optimal. The SCSO balances the exploration and exploitation phases through the use of the $\overrightarrow{R}$ parameter in Eq. (2), which decreases magnitude from $2 \rightarrow 0$ linearly while assuming parameter $S_M = 2$. The position of each search agent is updated in each iteration, and the distance between the agent's current and best positions is calculated. Eq. (3) balanced the phase transition and Eq. (5) elaborates avoiding local optimum trapping. During each iteration, the best candidate position $\overrightarrow{Pos_c}$ updated together with current position $\overrightarrow{Pos_c}$ followed by the sensitivity range $\overrightarrow{r}$. The direction of movement is determined through a random angle $\theta$ within a range of $0$–$360°$, selected through a roulette wheel mechanism. The optimal solution is approached by the search agents through circular movement in the SCSO algorithm. $\overrightarrow{Pos_b}$ and $\overrightarrow{Pos_{rnd}}$ are the best solution and the random position in Eq. (5).

$$\overrightarrow{r_G} = S_M - \left( \frac{s_M \times iter_c}{iter_{Max}} \right) \tag{1}$$

$$\overrightarrow{R} = 2 \times \overrightarrow{r_G} \times rand\,(0,1) - \overrightarrow{r_G} \tag{2}$$

$$\overrightarrow{r} = \overrightarrow{r_G} \times rand\,(0,1) \tag{3}$$

$$\overrightarrow{Pos}^{(t+1)} = \overrightarrow{r} \cdot \left( \overrightarrow{Pos_{bc}}^{(t)} - rand\,(0,1) \cdot \overrightarrow{Pos_c}^{(t)} \right) \tag{4}$$

$$\overrightarrow{Pos_{rnd}} = \left| rand\,(0,1) \cdot \overrightarrow{Pos_b}(t) - \overrightarrow{Pos_c}^{(t)} \right| \tag{5}$$

$$\overrightarrow{Pos}^{(t+1)} = \overrightarrow{Pos_b}(t) - \overrightarrow{r} \cdot \overrightarrow{Pos_{rnd}} \cdot \cos(\theta) \tag{6}$$

$$\overrightarrow{X}(t+1) = \begin{cases} \overrightarrow{Pos_b}^{(t)} - \overrightarrow{r} \cdot \overrightarrow{pos_{rand}} \cdot \cos(\theta) & |R| \le 1; exploitation \\ \overrightarrow{r} \cdot \left( \overrightarrow{Pos_{bc}}^{(t)} - rand\,(0,1) \cdot \overrightarrow{Pos_c}^{(t)} \right) & |R| \le 1; exploitation \end{cases} \tag{7}$$

### 2.2. Reinforcement learning (RL)

There are several techniques involved in Machine Learning (ML), such as Supervised Learning, Unsupervised Learning, Semi-supervised Learning, and Reinforcement Learning [43]. RL algorithms aim to train an agent in a complex environment to learn optimal actions. The agent's training involves performing diverse tasks in varying environments by receiving feedback from observing the environment. The effectiveness of the agent is enhanced through various methods. The interaction of the agent with its environment is a vital element of the system structure [44]. The use of Machine Learning algorithms has increased suggestively in recent years to resolve problems [45–47].

RL is one of the four branches of ML and involves placing an agent in a complex environment to learn optimal actions. There are two types of RL methods: model-free and model-based. Model-free methods can be further subdivided into two groups: value-based and policy-based strategies.

The reinforcement agent in value-based RL algorithms obtains knowledge from its actions and experiences in the environment and utilizes this information to make decisions based on the success of its actions and the rewards or penalties it receives. Q-Learning is a well-known value-based RL algorithm that involves assigning random actions to the agent and updating a Q-Table to determine the best action to
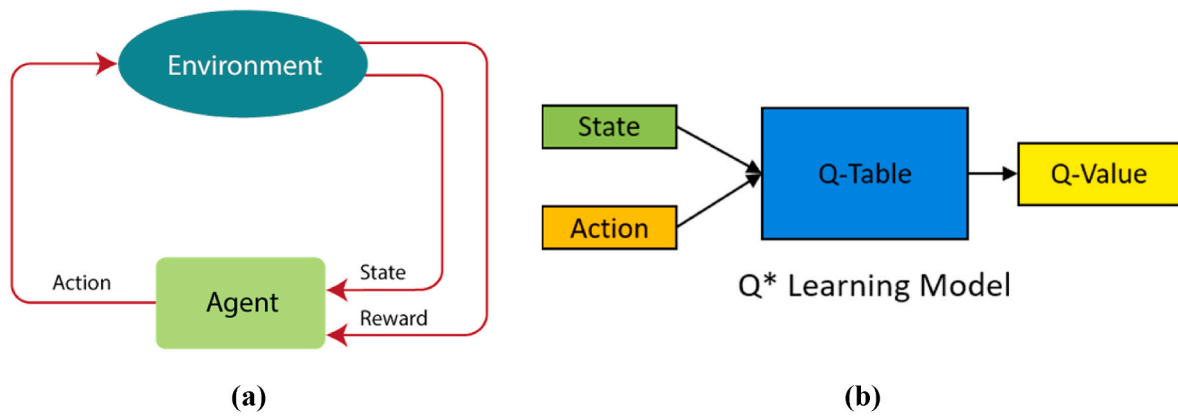
**Fig. 1.** Reinforcement Q-learning: Agents and Environments (a) Information flow (b) State flow.
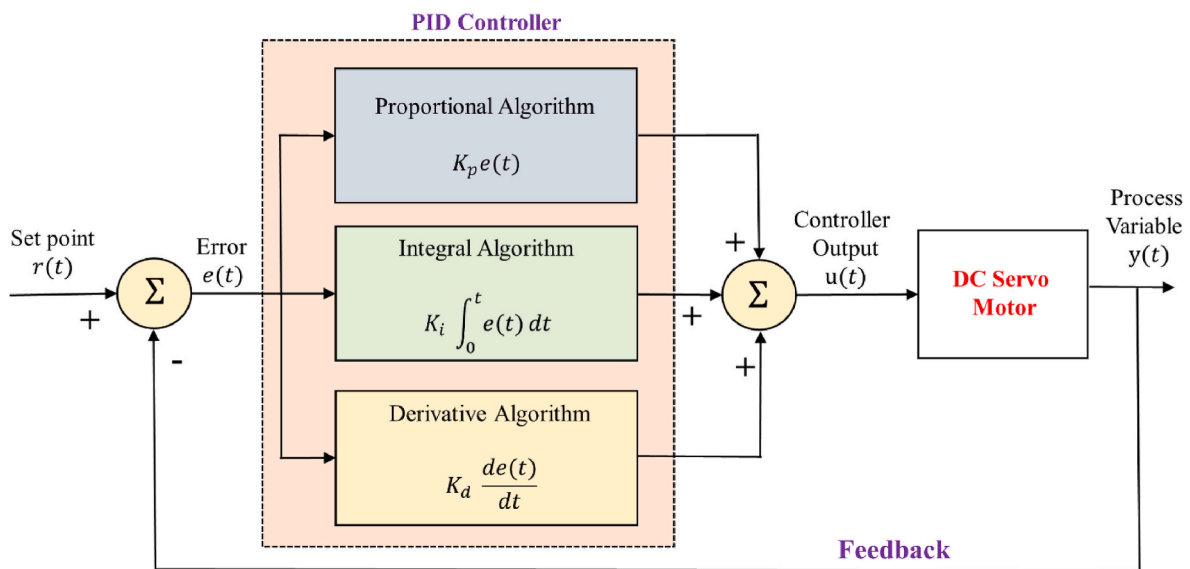


**Fig. 2.** A PID controlled DC motor speed system.

take based on the resulting rewards/penalties. The agent then decides whether to explore or exploit the environment [48].

### 2.3. Q learning based SCSO algorithm (QSCSO)

This study employs metaheuristic algorithms to solve problems by offering answers that are close to the best solutions while using less computational power. A comprehensive and precise description of the problem is needed to achieve this. Each metaheuristic technique has its own advantages and disadvantages, but this study aims to provide an inclusive and precise strategy by considering a larger set of parameters.

This study proposes a hybrid algorithm that combines the Q-learning algorithm, a value-based reinforcement learning approach, with metaheuristic algorithms. The choice of Q-learning is due to its compatibility with metaheuristics and ease of use in collaboration with them [49]. In Q-learning, the primary aim of the agent is to update its state by taking actions that lead to the highest Q-value. The optimal state is determined based on the benefits yielded by each potential state. Based on its actions, the agent is either rewarded or penalized at each step. The Q-Table is updated using the Bellman Eq. (8) and prepared for the next episode. Fig. 1 provides an overview of the general architecture of reinforcement learning agents and environments.

$$Q_{t+1}(s_t, a_t) \leftarrow Q_t(s_t, a_t) + \lambda \left[ r_{t+1} + \gamma \, Max \, Q_{t(s_{t+1}, a)} - Q_t(s_t, a_t) \right] \quad (8)$$

The equation in the Q-Learning algorithm involves the current state ($s_t$), the next state ($s_{t+1}$), and the current action ($a_t$). The learning rate is represented by $\lambda$ and the discount factor is represented by $\gamma$ whose magnitude varies from 0 to 1 that control the speed of the learning process and the significance of future rewards, respectively. The immediate reward or penalty received for taking a current action is used to update the Q-Table shown in Fig. 1 (b). The Q-Table, along with the Reward Table and the Bellman equation, are the fundamental components of the Q-Learning algorithm that work together to solve a problem.

The Q-Learning algorithm utilizes the concept of penalizing or rewarding an agent based on its state/action composition. The Q-Table matrix acts as a representation of an agent's experiences and initially, all values in the matrix are set to zero. The Q-Table matrix is continually updated with the Bellman equation after each iteration/ episode in a bid to create a probability equation that can help evaluate each potential state and the corresponding action from that state. In this regard, the proposed framework involves defining both the reward table and the Q-table as two-dimensional matrices, which can aid in making informed decisions during exploration and exploitation activities. The SCSO algorithm, which features a parameter denoted as "R," is employed to control the balance between exploration and exploitation. When the value of |R| is less than 1, the algorithm exploits, and it explores when |R| is greater than 1. The RLSCSO algorithm utilizes the |R| parameter to manage the Q-values, which play a vital role in
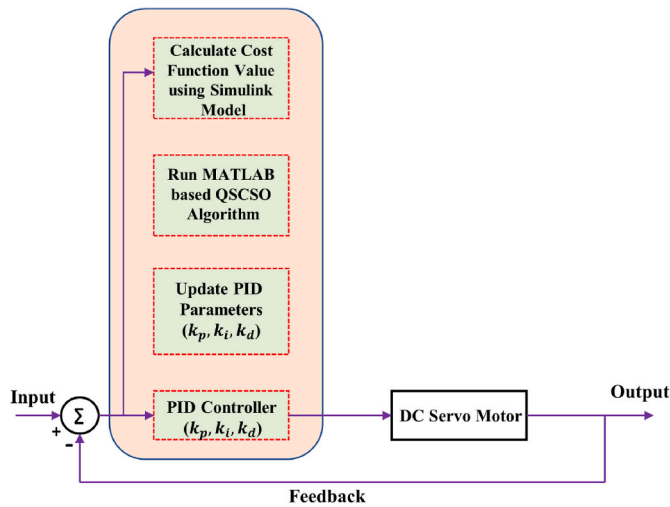
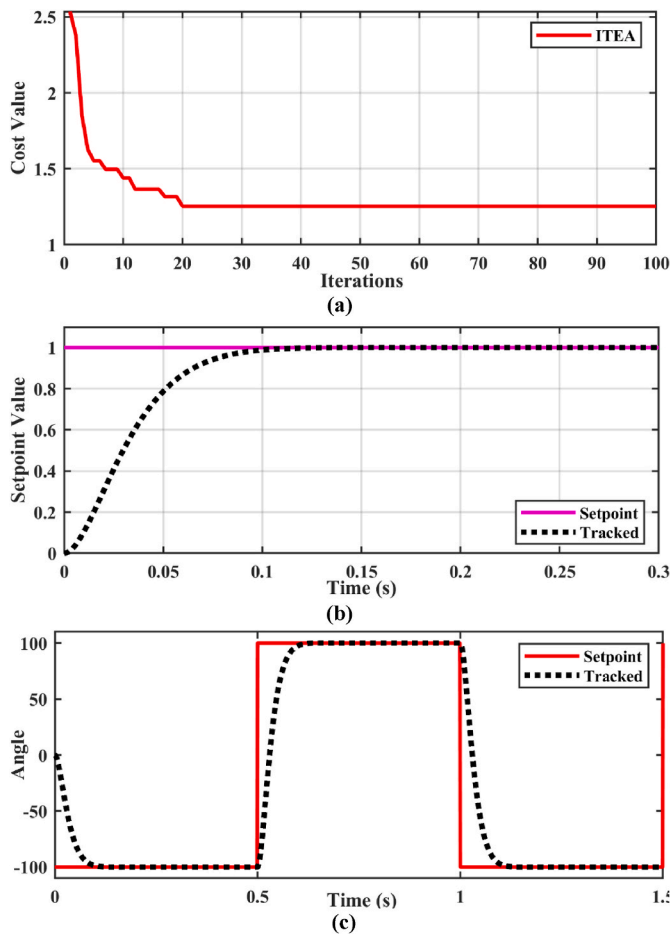**Fig. 3.** QSCSO based PID tuning system for DC servo motor.



**Fig. 4.** Set point tracking by PID (a) loss function over training iteration (b) STC setpoint tracking (c) varying setpoint tracking.

determining the best decision for both exploration and exploitation. A fitness function is employed to guide the appropriate decision-making process, and the algorithm continues until the optimal solution is achieved. The RLSCSO approach leverages both the |R| and Q-values to control the fitness function, and there are two mechanisms used to update the position: the conventional SCSO position update and the learning-based position update. The latter mechanism contains learning

values. The proposed method in this study includes a unique feature that sets it apart from other similar methods, its capability to alternate between exploration and exploitation phases as needed. This enhances its effectiveness in finding solutions by exploring the search space more efficiently and rapidly discovering the best solutions in a shorter amount of time and with fewer iterations compared to other metaheuristic algorithms. The final position updation is done using Eq. (9)

$$\overrightarrow{X}(t+1)=\begin{cases} \sigma \cdot \overrightarrow{Pos_b}(t) - \overrightarrow{r} \cdot \overrightarrow{Pos_{md}} \cdot \cos(\theta) & |R| \leq 1; exploitation \\ \sigma \cdot \overrightarrow{r} \cdot \left( \overrightarrow{Pos_{bc}}(t) - rand(0,1) \cdot \overrightarrow{Pos_c}(t) \right) |R| > 1; exploration \end{cases}$$

$$(9)$$

where |R| controls the position updating balance with respect to exploitation and exploration.

### 2.4. PID controller

The regulation of speed was accomplished through the manipulation of armature voltage. A closed loop control system, utilizing a PID controller, was depicted in Fig. 2. The PID controller is represented by the transfer function in Eq. (10), where $K_p$, $K_i$, and $K_d$ are the proportional, integral, and derivative gains, respectively. The variables $\omega$ and $\omega_{ref}$ represent the actual motor speed in addition to the reference speed, respectively.

$$G_{PID}(s) = K_P + \frac{K_i}{S} + K_d s \tag{10}$$

The open-loop transfer function of a DC motor can be derived as follows: The relationship between the induced voltage and the angular velocity is given by:

$$e_b(t) = K_P \frac{d\theta(t)}{dt} = K_b \omega(t) \tag{11}$$

where $K_b$ is the electromotive force constant, $e_b(t)$ is induced voltage due to a flux which is constant proportional to the angular velocity $\omega(t)$ which is given by the derivative of the position with respect to time, i.e., $d\theta/dt$. This relationship forms the basis for the open-loop transfer function of a DC motor, which can be used to model its behavior in the absence of feedback control. The armature voltage ($e_a(t)$) is a key parameter in the control of the speed of an armature-controlled DC servo motor. The behavior of the armature circuit can be described by a differential Eq. (12). This equation relates the armature voltage, current, and the mechanical position of the motor. Model is utilized to study the response of the motor for various inputs and disturbances. By analyzing the armature circuit's differential equation, the dynamic behavior of the motor can be predicted and its performance can be improved by design or by feedback control.

$$e_a(t) = L_a \frac{di_a(t)}{dt} + R_a i_a(t) + e_b(t) \tag{12}$$

Under the assumption that the load torque is zero, the torque produced by the armature current is determined by the sum of the inertia and friction torques. This relationship is given by Eq. (13). The torque produced by the armature current is an important parameter in the control of the DC servo motor, as it determines the dynamic response of the motor to changes in the armature current. By analyzing this relationship, the performance of the motor can be optimized for a given set of operating conditions, such as speed or position control. The torque-current relationship is also a key component in the design of feedback control systems for the DC servo motor, as it can be used to design controllers that ensure stable and accurate performance.

$$T(t) = J \frac{d\omega(t)}{dt} + B\omega(t) = K_m i_a(t) \tag{13}$$

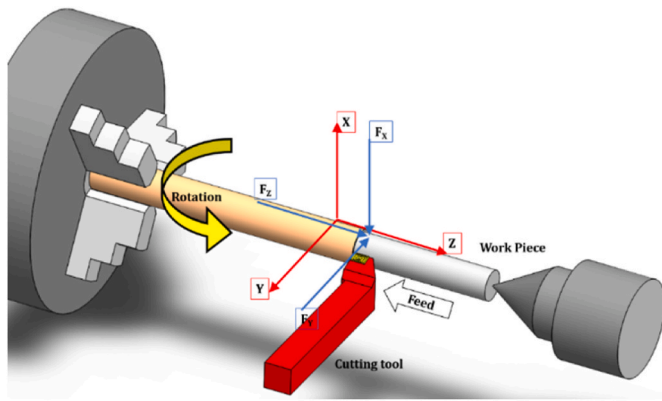Laplace transformation of Eq. 12 and 13 with Initial condition = 0,

**Fig. 5.** Machining model.

**Table 4**
Work-piece dimension specification.

| Length, mm | Diameter, mm | L/D, % |
|---|---|---|
| 200 | 20 | 10 |

**Table 5**
Tool specification.

| Description | Specification |
|---|---|
| Tool Holder | DCLNR 2020 K 12 |
| Insert | CNMG 12 04 08 |
| Nose radius | 0.8 mm |
| Coating | AlTiN |
| Insert type | Chip breaker |

**Table 6**
Machining parameters [53].

| Description | Specification |
|---|---|
| RPM | 250 |
| Feed rate, mm/rev. | 0.06 |
| Max. Cutting depth, mm | 0.25 |
| Amplitude of vibrations (without contact), $\mu m$ | 0.637 |

are given by Eq. 14–16

$$E_b(s) = K_b\Omega(s) \tag{14}$$

$$E_b(s) = (L_a s + R_a)I_s(s) + E_b(s) \tag{15}$$

$$T(s) = (Js + B)\Omega(s) = K_m I_a(s) \tag{16}$$

Based on the previous relationships, the open-loop transfer function describing the relationship between the input voltage and the output speed of a DC motor can be written as in Eq. (17). By analyzing the open-loop transfer function, the response of the motor to various inputs and disturbances can be predicted and its performance can be improved by design or by feedback control.

$$\frac{\Omega(s)}{E_a(s)} = \frac{K_m}{(L_a s + R_a)(Js + B) + K_b K_m}, for\ T_{Load} = 0 \tag{17}$$

This transfer function models the behavior of the DC motor when it is subjected to an external load torque and no input voltage is applied.

$$\frac{\Omega(s)}{T_{Load}(s)} = \frac{(L_a s + R_a)}{(L_a s + R_a)(Js + B) + K_b K_m}, for\ E_a = 0 \tag{18}$$

where the affiliation between the motor speed ($\omega$) and the load torque ($T_{Load}$) when the input voltage ($E_a$) is "zero" can also be represented by a transfer function.

### 2.5. Proposed QSCSO based PID controller

The proposed QSCSO algorithm has specific parameters, which are listed in where t 0 is the initial time, $t_{sim}$ is the final time, t is the instantaneous time and e(t) represents the absolute error magnitude at time *t*. The ITAE metric provides a weighted measure of the system's response, giving greater emphasis to errors that occur earlier in dynamic control action. The ITAE provides the better optimization control tuning parameters of the PID controller with enhanced system's performance and reduce oscillations.

The block diagram of the QSCSO-based PID (QSCSO-PID) controller for the DC motor is shown in Fig. 3 The ITAE function is commonly used as an objective function in the design of PID controllers, as it provides a measure of the performance of the controller in terms of the error between the reference signal and the actual output. The use of the ITAE function in combination with the QSCSO-PID controller is aimed at improving the performance of the DC motor control system. The block diagram of the QSCSO-PID controller provides a visual representation of the control system and can be used to understand the different components and their interactions in the control loop. The ITAE (Integral of Time-weighted Absolute Error) function was used in the study as a performance measure for comparison with previous works as referenced in Ref. [50]. The ITAE objective function [51] is described by Eq. (19) (see Fig. 4).

$$ITAE = \int_0^{t_{sim}} t.\ |e(t)|dt \tag{19}$$

where $t_0$ is the initial time, $t_{sim}$ is the final time, $t$ is the instantaneous time and $e(t)$ represents the absolute error magnitude at time $t$. The ITAE
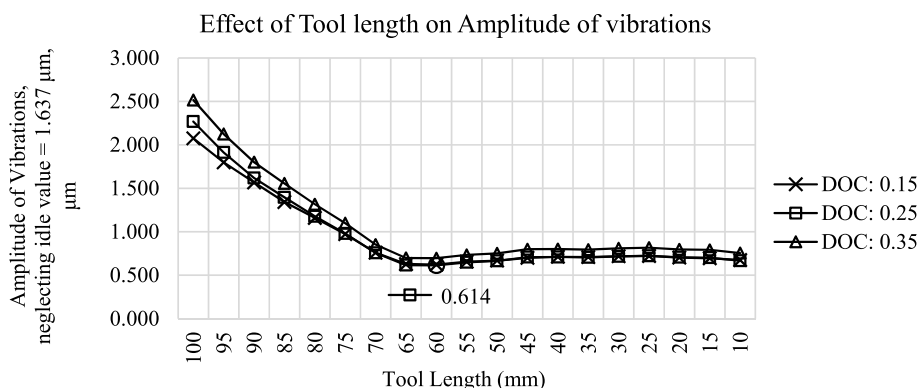


**Fig. 6.** Trend of Tool length w.r.t. Amplitude of vibrations.
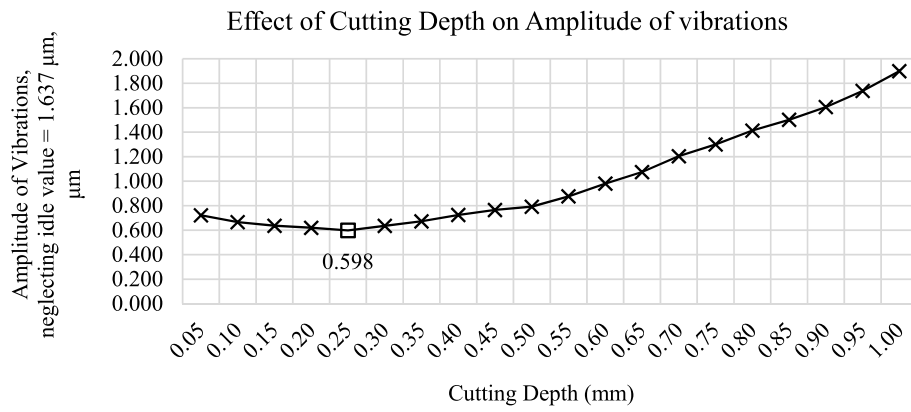
Fig. 7. Trend of cutting depth w.r.t. amplitude of vibrations.
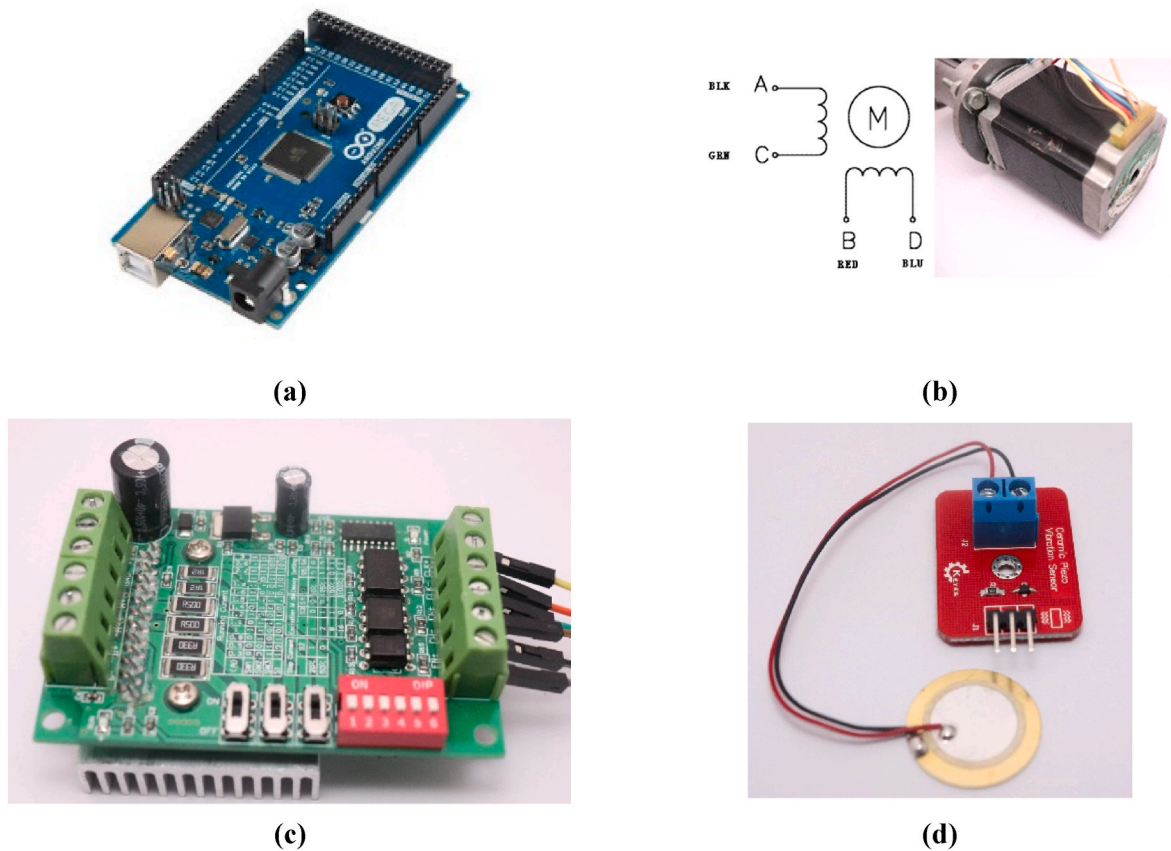


**(a)**



**(b)**



**(c)**



**(d)**

**Fig. 8.** (a) Arduino Mega. (b) Nema 23 stepper motor. (c) TB6065 single axis motor driver. (d) Ceramic piezo-electric vibration sensor.



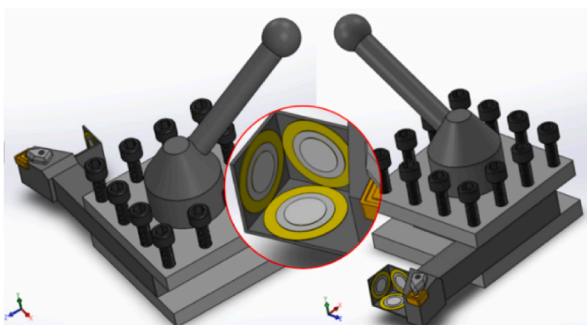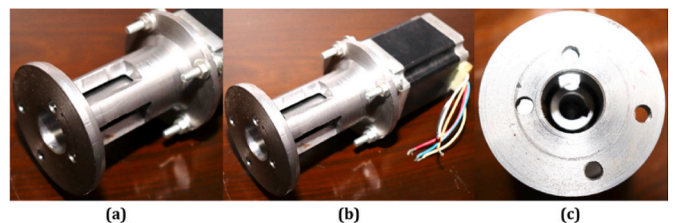**Fig. 9.** Sensor placement scheme.



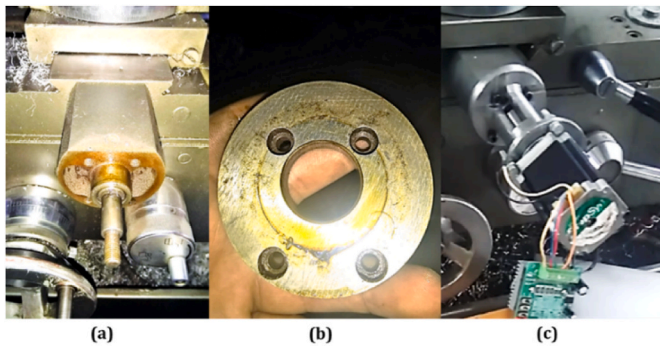**Fig. 10.** Jig designed to hang motor. (b) Jig attached with motor. (c) Jig and Shaft Coupling.

**Fig. 11.** (a) Knob detached from the cross slide assembly. (b) Reading flange for the correct design of jig. (c) Motor hanged with the cross slide assembly and shaft of motor coupled with the lead screw of cross slide.

metric provides a weighted measure of the system's response, giving greater emphasis to errors that occur earlier in dynamic control action. The ITAE provides the better optimization control tuning parameters of the PID controller with enhanced system's performance and reduce oscillations.

The process of optimizing the gains of a PID controller using the QSCSO algorithm begins with the integration of a MATLAB/Simulink model for DC motor speed control and the QSCSO algorithm. The PID gains to be optimized are represented as a vector of real numbers, P, i-e., $P = [K_p ; K_i ; K_d]$. A population of N randomly generated gas particles and their oppositions is created. The proposed PID controller and unity feedback system for the DC motor's speed control is simulated in the time domain for each gas particle. The resulting speed response curves and ITAE (Integral of Time-weighted Absolute Error) values are obtained. The QSCSO algorithm is used to update the PID gains. The algorithm models the social behavior of the particles with a Gaussian

distribution and the gas behavior of the particles with the ideal gas law. During each iteration, the velocity and acceleration of the gas particles are updated based on the velocity and best particle information of the entire population. The algorithm terminates when a specified condition is met, such as reaching a maximum number of iterations or a certain level of accuracy in the ITAE value. The resulting optimal PID gains can then be utilized to improve the performance of the DC motor speed control system.

During the optimization process, it is typical to obtain varying speed output curves and ITAE values across different particles. To determine the optimal solution, the N particles with the lowest ITAE values are identified and updated for the subsequent iteration before the HGSO algorithm is resumed. Oppositions are generated while each gas particle is being updated, leading to a bidirectional flow between the control system and the QSCSO algorithm. This process continues until the maximum iteration is reached. The gas particle with the lowest ITAE value is then considered the optimal set of PID controller gains. The flow chart of the proposed design procedure is shown in Fig. 3, which summarizes the entire optimization process using the QSCSO algorithm for finding the optimal PID gains.

## 3. Experimental setup

Conferring From previous studies, opting cutting depth as a control parameter among various parameters, utilizing standard tooling for machining and OEM set parameters, vibration amplitude range is gauged using standard industrial equipment for specified conditions [52]. Fig. 1 displays the fundamental machining model used to calibrate the Arduino-based intelligent machining setup. The performance of the setup was evaluated by machining different materials and verifying their conformance with the designed setup. The prerequisites for the experimentation were first determined.

AISI420 has a wide variety of applications in pressurized equipment
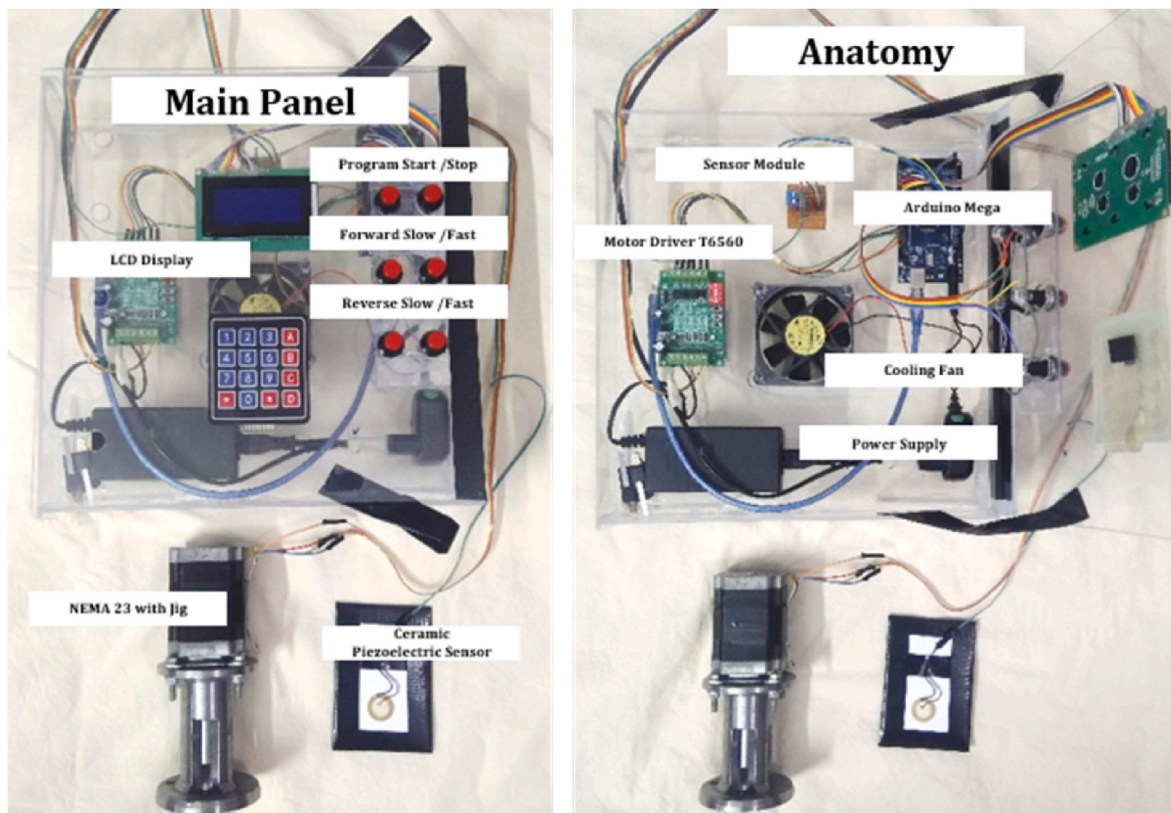


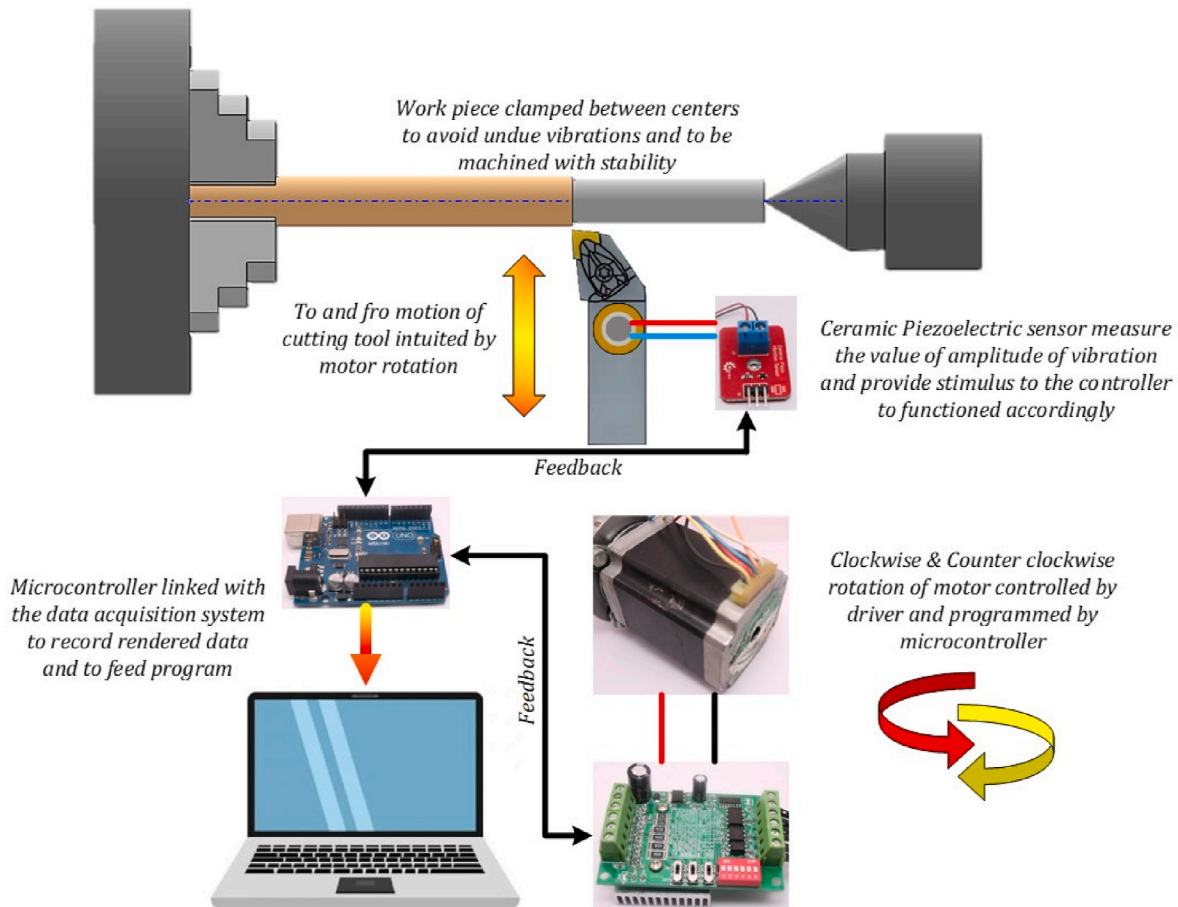**Fig. 12.** Arduino based intelligent machining setup.

**Fig. 13.** Schematic diagram of the designed experimental setup.

**Table 7**

Alteration in least count of cross slide.

| Parameter Explanation | Value |
|---|---|
| Least count of cross slide without stepper motor | 0.1 *mm* reduction in diameter |
| Least count of cross slide with stepper motor (step: 1.8°) | 0.025 *mm* reduction in diameter |

and machinery, for cutting, surgical and aerospace industry because of its high strength when hardened and high formability when annealed. Whereas many issues arise regarding surface finish during machining when annealed and almost impossible when hardened. That is why starting from AISI420 work-piece in order to achieve more focused results while analyzing amplitude of vibrations, having following physical and chemical properties.

Whereas the specification of arbitrarily selected long work-piece is as follows. Tool is selected based on OEM recommendation, while machine tool is selected as per availability.

Recommended machining parameters for selected tool w.r.t. work-piece material is given by Table 4 and 5 as follows.

Selected tool being optimally designed has not considerable effect on amplitude of vibrations measured through industrial on-field analyzer. In order to refine as much as possible starting from maximum over hanged length, following trend is depicting the outcome, such that lowest amplitude of vibrations occurred while tool length is 60 mm over hanged. Considering the assessed tool length as another fixed parameter while varying cutting depth. Starting from 0.05*mm* depth of cut, and with an increment of 0.05*μm* on separate samples. Measured amplitude of vibrations corresponding to each sample recorded an optimum

threshold (0.598*μm*) in following Plot.

## 4. Embedded system based intelligent machining setup

Microcontroller has completely changed the esthetics of machine, that is why Arduino is used to aid the set goal. Complete developed machining unit comprises of four elements; Arduino MEGA to control intelligently, NEMA 23 stepper motor to move axis, TB6065 single axis motor driver and Ceramic piezo-electric vibration sensor module for Arduino. The system is based on the simple logic "*to control the cutting depth while increase or decrease in amplitude of vibration*" (see Table 6).

Schematics of the machining setup is developed in such a way that the standard tool is modified (attachment weighs only 22 g, negligibly affecting the structure) in order to place three vibration sensors to measure amplitude of vibrations along orthogonal axis whereas clamped on same over hanged length of 60 mm as shown in Fig. 8. Only one minor alteration is made on lathe machine that the knob of cross slide is replaced with a specially design jig in order to couple motor with the cross slide as shown in Figs. 10 and 11. All the components are assembled in a console box having LCD for display of amplitude of vibrations and buttons to start/stop the program and to manually control the tool approach as shown in Fig. 12. The complete illustration of the machining setup and schematic diagram is shown in Figs. 13 and 14. Moreover, alteration increases accuracy in cutting depth described in Table 7.

The present study employed a cost-effective ceramic piezoelectric sensor as a sensing module due to its high responsiveness. The sensor generated electrical signals were calibrated in accordance with the corresponding vibration amplitude. Although the sensor is inherently insensitive to the axial direction of force, three sensors were utilized
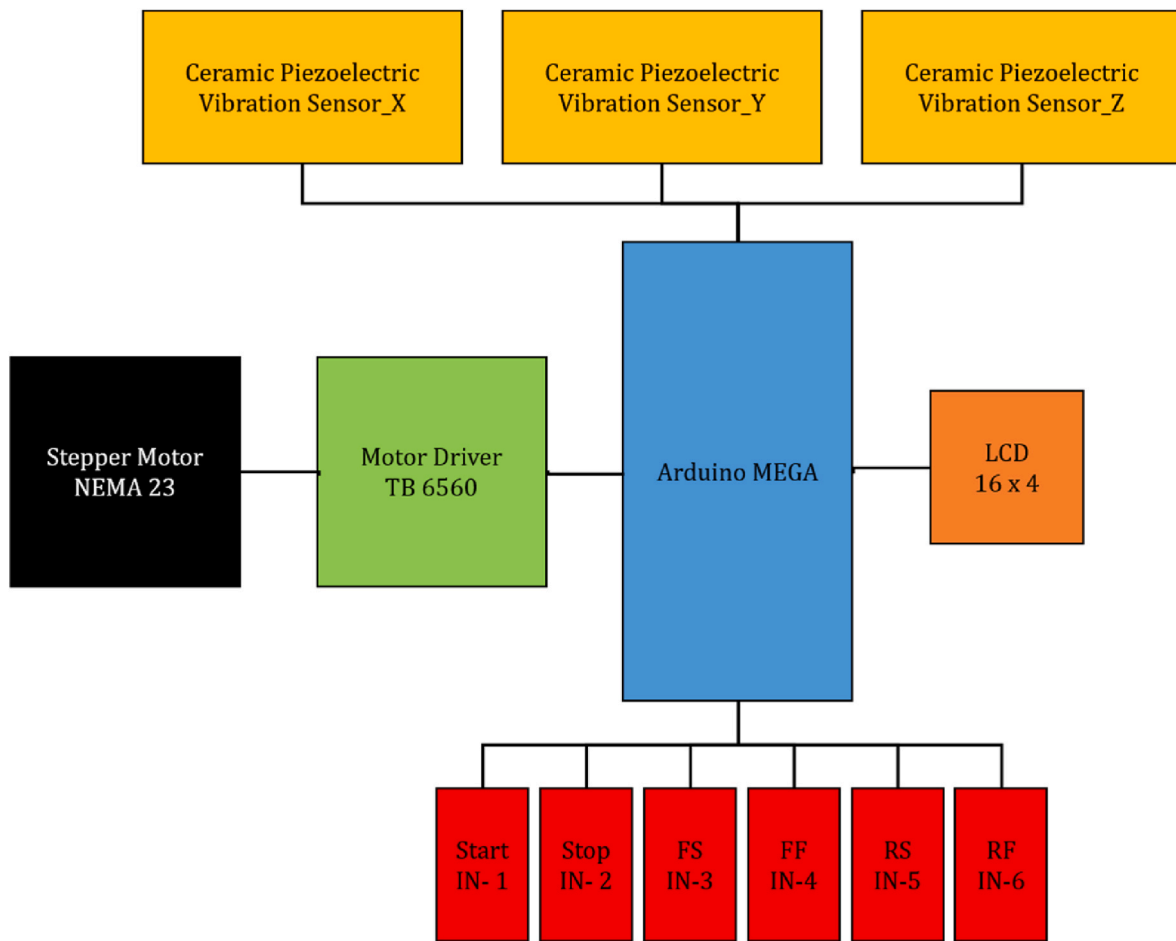
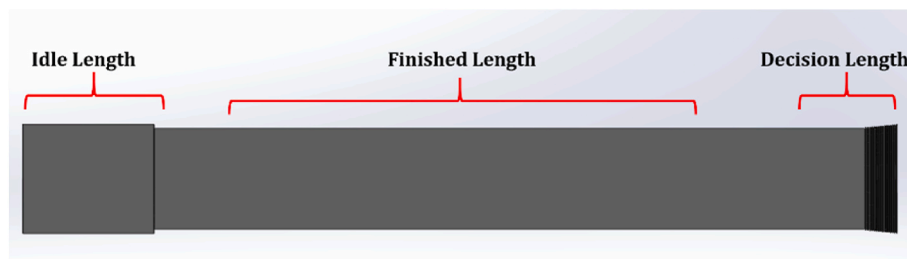**Fig. 14.** General representation of Circuitry.



**Fig. 15.** Work-piece partition as per machining performed (Programming Mode – II).
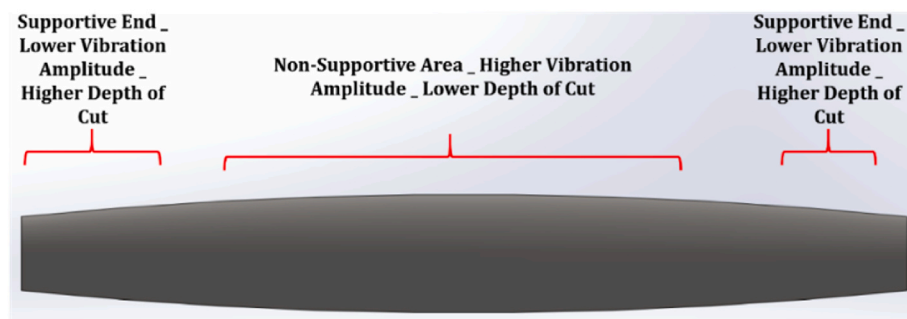


**Fig. 16.** Programming mode – I.

**Table 8**
Comparison of two programming modes.

| Material sample | Programming Mode – I | Programming Mode – II |
|---|---|---|
|  **AISI420 (25–30 HRC)** | TRIMOS   DH-8<br>HW: 1.00   SW: 1.08   NR: 01166<br>Name: \_\_\_\_ AISI 420 Samp1-1 \_\_\_\_<br>Drawing: _____<br>11.12.2019   12:04:55<br>Lt=15.0   Lc=2.50 mm   P2<br>Ra = 1.212 μm<br>Rz = 8.726 μm<br>Rmax = 9.696 μm | TRIMOS   DH-8<br>HW: 1.00   SW: 1.08   NR: 01166<br>Name: \_\_\_\_ AISI 420 Samp1-2 \_\_\_\_<br>Drawing: _____<br>02.01.2020   14:45:05<br>Lt=15.0   Lc=2.50 mm   P2<br>Ra = 1.227 μm<br>Rz = 8.834 μm<br>Rmax = 9.816 μm |
| Depth of cut | *variable* | 0.237 *mm* |
| Dimension from the middle of finished length, ∅ | 19.784 *mm* | 19.763 *mm* |
| Surface finished value, $R_a$ | 1.212 *μm* | 1.227 *μm* |

along the x, y, and z-axes as presented in Fig. 9. The composite response of these sensors was then utilized since minor differences in the amplitude values were observed in different axial directions. Furthermore, it was noticed that the distance between the cutting edge and the sensor had a significant impact on the response value. Hence, the experimental setup was designed in such a way that the sensor was positioned as close to the cutting edge as possible, within the constraints of the available resources (see Fig. 6).

The whole experimentation depends on how well the sensors are calibrated according to specified scenario. The threshold value of amplitude of vibration found out to be 0.598 $\mu m$ or 0.6$\mu m$ as previously described. Sensor is calibrated such that without contact sensor must measure 0.0598 $\mu m$ and should follow the same plot in Fig. 7. The circuitry is represented in Fig. 13 and the logic diagram based on which the coding works as per designed criterion in presented in Fig. 14.

Sensor enabled the motor rotation counter-clockwise or clockwise when amplitude of vibration fall or rise from set threshold respectively, allowing the to and from movement of tool. The machining performed by the setup is described in Fig. 15. Idle length is the clamping portion whereas the decision length is the portion where sensor maintained the set amplitude of vibration and fixed the respective cutting depth throughout the specified cut. The results are only compared to the portion of finished length.

The setup executed machining by programming in two ways. In first mode presented in Fig. 16 has proven high surface finish and low dimensional accuracy in which amplitude of vibration remains constant whereas cutting depth varies, while second mode presented in Fig. 14 has proven low surface finish and high dimensional accuracy in which amplitude of vibration varies whereas cutting depth remains constant.

Comparison of machining using two programming modes is shown in Table 8 for several sample materials. Mode – I has 21 $\mu m$ more dimensional variation as compared to Mode – II, whereas Mode – II has difference of 0.015 $\mu m$ w.r.t. Mode – I in surface finish. Considering difference of surface finish negligibly small Mode – II is more dimensionally accurate, hence recommended.

Study has revealed that Arduino based intelligent machining setup is independent of material length, diameter and hardness of the material while keeping material and tool related OEM's recommended parameters constant, machining setup controls cutting depth whereas maintaining amplitude of vibrations to the set limit. Proceedings of experimentation has developed an empirical relationship between the amplitude of vibrations and surface finish of work-piece;

$$V^c = \left(V^a - V^i\right) \times 2 \tag{20}$$

Comparison of surface roughness $R_a$ is as;

$$\% \text{ Error w.r.t. } V^c = \frac{R_a - V^c}{R_a} \times 100 \tag{21}$$

$$\% \text{ Error w.r.t. } V^o = \frac{R_a - V^o}{R_a} \times 100 \tag{22}$$

where value of vibration amplitude measured by vibration analyzer = $V^a$ (magnitude of vibration) measured by vibration analyzer in idle condition at $V^i$ = 1.637 μm, comparison value calculated by vibration analyzer = $V^c$. Comparison value measured by Arduino based machining setup = $V^o$. Experimentation is performed on different variety of materials and results are summarized in Table 9. Considering 25–30 mm clamping portion, 25–30 mm decision portion, samples are cut down to the length of 100 mm and only the center portion of finished length about 50 mm is compared for good conformance.

## 5. Results and discussions

The amplitude of vibration is dependent upon the machining parameters such as spindle speed, feed rate, cutting depth, material of work-piece, geometry and type of cutting tool as well as Length of tool. Optimization required algorithmic study whereas standard tooling can refer to the OEM's design data. The trend shown in Fig. 7, commits the trueness of the process for the specified condition only. Therefore, the value of amplitude of vibrations was found to be 0.614 μm against the over hanged length of tool, which is 60 mm while neglecting the value 1.637 μm (value without contact of tool and work-piece).

For the optimization of the cutting depth all other parameters were kept fixed, which were gathered from standard literature. Whereas by varying the cutting depth, the corresponding amplitude of vibration was recorded from the standard industrial vibration analyzer and plotted accordingly shown in Fig. 8. The minimum value of vibration amplitude was recorded to be 0.598 μm against the cutting depth 0.25 mm. It seems that larger the cutting depth greater will be the amplitude of vibration. Well, it was found true for the cutting depth greater than 0.25 mm, but it was contrary for the cutting depth less than 0.25 mm. by applying cut of only 0.05 mm the amplitude of vibration was recorded about 0.721 μm, which will definitely produce poor surface finish as compared to the true one. The reason for this is because tool experiences reaction forces from the work-piece, which sometimes aids to damp the vibrations when the forces cancel the reaction effect. Therefore, the cutting depth less than 0.25 mm does not cancels the reaction forces effect and hence, produce larger amplitude of vibrations.

Amplitude of vibration was made optimum, by employing optimum tool length and optimum cutting depth. Arduino based machining setup intelligently serves this purpose. Already controlled cutting length, system controlled only cutting depth and amplitude of vibrations as a feedback loop function. The developed setup differs from the advanced machining setups due to simplicity of design and ease to use in Arduino ISE. The compatibility to all conventional machine tools is undertaken considering the cost effective too.

**Table 9**
Comparison of different materials vibration amplitude w.r.t. surface finish.

| Sample | | | | Surface Finish Value $R_a$, μm |
|---|---|---|---|---|



AISI420 (25–30 HRC)

```
TRIMOS              DH-8
HW: 1.00    SW: 1.08    NR: 01166

Name:        AISI 420 Samp1-2

Drawing:

02.01.2020        14:45:05
Lt=15.0    Lc=2.50 mm          P2
Ra     =    1.227    μm
Rz     =    8.834    μm
Rmax   =    9.816    μm
```

| $V^c = (V^a - V^i)x2$, μm | $V^o$, μm | % Error w.r.t. $V^c$, $\dfrac{R_a - V^c}{R_a}$ x 100 | % Error w.r.t. $V^o$, $\dfrac{R_a - V^o}{R_a}$ x 100 |
|---|---|---|---|
| 1.208 | 1.2 | 1.5% | 2.2% |



AA6061 T6 (55–65 HRB)

```
TRIMOS              DH-8
HW: 1.00    SW: 1.08    NR: 01166

Name:          Alu Samp2

Drawing:

02.01.2020        14:51:21
Lt=15.0    Lc=2.50 mm          P2
Ra     =    1.311    μm
Rz     =    9.503    μm
Rmax   =    10.65    μm
```

| $V^c = (V^a - V^i)x2$, μm | $V^o$, μm | % Error w.r.t. $V^c$, $\dfrac{R_a - V^c}{R_a}$ x 100 | % Error w.r.t. $V^o$, $\dfrac{R_a - V^o}{R_a}$ x 100 |
|---|---|---|---|
| 1.269 | 1.2 | 3.2% | 8.4% |



AISI 1045 (20–25 HRC)

```
TRIMOS              DH-8
HW: 1.00    SW: 1.08    NR: 01166

Name:          MS Samp4

Drawing:

02.01.2020        15:11:04
Lt=15.0    Lc=2.50 mm          P2
Ra     =    1.291    μm
Rz     =    9.295    μm
Rmax   =    10.32    μm
```

| $V^c = (V^a - V^i)x2$, μm | $V^o$, μm | % Error w.r.t. $V^c$, $\dfrac{R_a - V^c}{R_a}$ x 100 | % Error w.r.t. $V^o$, $\dfrac{R_a - V^o}{R_a}$ x 100 |
|---|---|---|---|
| 1.223 | 1.2 | 5.3% | 7.0% |



AISI 316 (20–25 HRC)

```
TRIMOS              DH-8
HW: 1.00    SW: 1.08    NR: 01166

Name:          SS Samp3

Drawing:

02.01.2020        14:59:38
Lt=15.0    Lc=2.50 mm          P2
Ra     =    1.238    μm
Rz     =    8.913    μm
Rmax   =    9.904    μm
```

| $V^c = (V^a - V^i)x2$, μm | $V^o$, μm | % Error w.r.t. $V^c$, $\dfrac{R_a - V^c}{R_a}$ x 100 | % Error w.r.t. $V^o$, $\dfrac{R_a - V^o}{R_a}$ x 100 |
|---|---|---|---|
| 1.217 | 1.2 | 1.7% | 3.1% |



Pure Copper

```
TRIMOS              DH-8
HW: 1.00    SW: 1.08    NR: 01166

Name:          Cu Samp5

Drawing:

02.01.2020        15:18:09
Lt=15.0    Lc=2.50 mm          P2
Ra     =    1.306    μm
Rz     =    9.367    μm
Rmax   =    10.41    μm
```

| $V^c = (V^a - V^i)x2$, μm | $V^o$, μm | % Error w.r.t. $V^c$, $\dfrac{R_a - V^c}{R_a}$ x 100 | % Error w.r.t. $V^o$, $\dfrac{R_a - V^o}{R_a}$ x 100 |
|---|---|---|---|
| 1.251 | 1.2 | 4.2% | 8.1% |

(*continued on next page*)

**Table 9** (*continued*)



Aluminium Bronze

| $V^c = (V^a - V^i)x2$, µm | $V^o$, µm | % Error w.r.t. $V^c$, $\dfrac{R_a - V^c}{R_a}$ x 100 |
|---|---|---|
| 1.246 | 1.2 | 3.8% |

| % Error w.r.t. $V^o$, $\dfrac{R_a - V^o}{R_a}$ x 100 |
|---|
| 7.4% |

Phenolic Bakelite

| $V^c = (V^a - V^i)x2$, µm | $V^o$, µm | % Error w.r.t. $V^c$, $\dfrac{R_a - V^c}{R_a}$ x 100 |
|---|---|---|
| 1.284 | 1.2 | 3.3% |

| % Error w.r.t. $V^o$, $\dfrac{R_a - V^o}{R_a}$ x 100 |
|---|
| 9.6% |

Thermoplastic (D80 shore)

| $V^c = (V^a - V^i)x2$, µm | $V^o$, µm | % Error w.r.t. $V^c$, $\dfrac{R_a - V^c}{R_a}$ x 100 |
|---|---|---|
| 1.265 | 1.2 | 4.9% |

| % Error w.r.t. $V^o$, $\dfrac{R_a - V^o}{R_a}$ x 100 |
|---|
| 9.7% |

Following effects were experienced related to Amplitude of vibrations during turning process.

1. Larger the tool length, larger will be the amplitude
2. Larger the depth of cut, larger will be the amplitude of vibration
3. The diameter of the shaft gets smaller, amplitude of vibrations gets larger
4. Larger amplitude of vibrations produce poor surface finish

The Arduino based machining setup maintains the optimized value of amplitude of vibrations, which is 0.6 µm. In response, the system accomplish optimized value of cutting depth. And hence, helped in the better achievement of surface finish. Being the comparable values obtained after series of experiments, Machining of different materials was done and the recorded values of vibration amplitude was compared with the $R_a$ value of surface finish. The conclusion was drawn that the values of surface finish is almost 2 times the average of the values of amplitude of vibration along orthogonal directions. Therefore, while controlling amplitude of vibrations; actually surface finish was controlled at the same time.

This system has a prime importance to visualize real-time surface finish value of work-piece during tuning process with less than 10% error, without using high-fi expensive instrumentation. For the specified machine tool, cutting tool, specified material spindle RPM, feed rate, and cutting depth the above-mentioned outcomes were drawn. If the scenario changes, the whole environment of the experimentation will be changed and different compatible parameters will definitely give results differ from the current scenario.

## 6. Conclusion and future prospects

In conclusion, the proposed Metaheuristic Algorithm Based PID Control system with a piezoelectric sensor provides a novel approach to optimize cutting depth and surface finish in turning processes. The experimental results demonstrated the system's ability to handle variations in cutting conditions and tool wear and tear while achieving improved robustness and stability compared to traditional PID control methods. The system's ability to achieve lower Integral of Time-weighted absolute error (ITEA) and reduced machining errors shows promise for improving machining performance. The sustained minimum amplitude of vibration and $R_a$ value of the surface finish is found to be comparable to standard models with less than 10% error. The proposed system has been tested on a variety of materials with different hardness levels, including Phenolic Bakelite, Copper, Thermoplastic, and Stainless Steel, with excellent results. Proposed framework is an effective solution for various industrial applications, especially those that require high-precision machining with complex material properties. Overall, the proposed framework has demonstrated its potential to optimize machining parameters and improve the overall efficiency of the turning process. Minimum value of vibration amplitude achieved is 0.598 µm for cutting depth of 0.25 mm. The value of amplitude of vibrations is 0.614 µm against the over hanged length of tool of 60 mm. Considering it the initial idea for based design, following points provides a guideline for further aspects of research work in this study.

- Parametric study was done efficiently without using advanced algorithms. ANN and DOE can be used for the design of experiment,

and Genetic algorithm and AI – algorithm provides an opportunity to optimize multiple objectives

- In order to compete with the advance machining techniques such as UAT, it is required to replace the vibration sensor with the more accurate Tri-Axial vibration sensor in order to get accurate and transient values
- The experiment was performed using little amount of cutting fluid. Which means it is comparable to the dry condition, contrary to flood cooling strategy. In future study with the application of MQL better results can be achieved
- Mathematical model was not engaged for the calculation of design as well as machining parameters, in future model must be design such an efficient that can directly relates the experimental setup
- Mounting sensor was used in current scenario, use of more advanced sensors like laser or non-touch sensors provides a breakthrough for the new sight of research

In future the same system can be imbed in to the CNC turning machines, in order to study the effects on machining, without doing hectic programming or modeling work-piece.

- Only the cutting depth was controlled using the developed machining setup, the control of spindle cutting speed must be added to the system for the study of multi-objectives optimization
- Since the surface roughness value is comparable to the amplitude of vibration so it provides a sight to study different parameters by setting the surface finish fixed objective and optimize other. Moreover, it provides an opportunity to test on field surface roughness during machining without the use of expensive equipment. Increasing accuracy of the system leads towards the cost-efficient model.

The limitations of PID tuned by stochastic model is additional computational complexity, difficulty in determining objective function, lack of interpretability, limited applicability to nonlinear systems, and dependence on initialization.

## Credit author statement

**Abdul Muqeet:** Conceptualization, Methodology, Resources, and Project Administration. **Asif Israr:** Validation, Data Curation. Muhammad Hamza Zafar: Conceptualization, Formal Analysis, Investigation. **Majad Mansoor:** Visualization, Data Curation. **Naureen Akhtar:** Supervision, Funding Acquisition, Investigation. All authors were involved in the preparation and review of the original manuscript.

## Declaration of competing interest

The authors declare that they have no known competing financial interests or personal relationships that could have appeared to influence the work reported in this paper.

## Data availability

No data was used for the research described in the article.

## References

[1] R. Matsumura, I. Nishida, K. Shirase, Tool life prediction in end milling using a combination of machining simulation and tool wear progress data, Journal of Advanced Mechanical Design, Systems, and Manufacturing 17 (2) (2023). JAMDSM0025-JAMDSM0025.
[2] J. Jastrzębska, et al., Measurement and identification of translational static stiffness in workspace of a machine tool, Int. J. Adv. Des. Manuf. Technol. (2023) 1–8.
[3] V.O.A. Akbari, et al., Identification of in-process machine tool dynamics using forced vibrations in milling process, Int. J. Mech. Sci. 239 (2023), 107887.
[4] A.M. El-Tamimi, T.M. El-Hossainy, Investigating the machinability of AISI 420 stainless steel using factorial design, Mater. Manuf. Process. 23 (4) (2008) 419–426.
[5] M. Mia, et al., Intelligent optimization of hard-turning parameters using evolutionary algorithms for smart manufacturing, Materials 12 (6) (2019) 879.
[6] E.J. Kim, C.M. Lee, A study on the optimal machining parameters of the induction assisted milling with inconel 718, Materials 12 (2) (2019) 233.
[7] A. Aslan, Optimization and analysis of process parameters for flank wear, cutting forces and vibration in turning of AISI 5140: a comprehensive study, Measurement 163 (2020), 107959.
[8] H. Marko, et al., Turning parameters optimization using particle swarm optimization, Procedia Eng. 69 (2014) 670–677.
[9] N.V.S. Shankar, et al., Process parameter optimization for minimizing vibrations and surface roughness during turning EN19 steel using coated carbide tool, Mater. Today: Proc. 24 (2020) 788–797.
[10] W.H. Yang, Y.S. Tarng, Design optimization of cutting parameters for turning operations based on the Taguchi method, J. Mater. Process. Technol. 84 (1) (1998) 122–129.
[11] P. Sahoo, Optimization of turning parameters for surface roughness using RSM and GA, Advances in Production Engineering & Management 6 (3) (2011).
[12] W. Saleem, et al., Computational analysis and artificial neural network optimization of dry turning parameters—aa2024-t351, Appl. Sci. 7 (6) (2017) 642.
[13] V.I. Babitsky, V.K. Astashev, A.N. Kalashnikov, Autoresonant control of nonlinear mode in ultrasonic transducer for machining applications, Ultrasonics 42 (1–9) (2004) 29–35.
[14] R. Kishore, S.K. Choudhury, K. Orra, On-line control of machine tool vibration in turning operation using electro-magneto rheological damper, J. Manuf. Process. 31 (2018) 187–198.
[15] A. Miyake, et al., Chip control in turning with synchronization of spindle rotation and feed motion vibration, Precis. Eng. 53 (2018) 38–45.
[16] C. Zhang, et al., Effects of ultrasonic vibrations in micro-groove turning, Ultrasonics 67 (2016) 30–40.
[17] R. Zhang, P. Steinert, A. Schubert, Microstructuring of surfaces by two-stage vibration-assisted turning, Procedia CIRP 14 (2014) 136–141.
[18] Ç.V. Yıldırım, Investigation of hard turning performance of eco-friendly cooling strategies: cryogenic cooling and nanofluid based MQL, Tribol. Int. 144 (2020), 106127.
[19] M. Ukamanal, P.C. Mishra, A.K. Sahoo, Effects of spray cooling process parameters on machining performance AISI 316 steel: a novel experimental technique, Exp. Tech. 44 (1) (2020) 19–36.
[20] G.M.A. Acayaba, P.M.d. Escalona, Prediction of surface roughness in low speed turning of AISI316 austenitic stainless steel, CIRP Journal of Manufacturing Science and Technology 11 (2015) 62–67.
[21] R.W. Maruda, et al., Tool wear characterizations in finish turning of AISI 1045 carbon steel for MQCL conditions, Wear 372–373 (2017) 54–67.
[22] M.Y. Noordin, et al., Application of response surface methodology in describing the performance of coated carbide tools when turning AISI 1045 steel, J. Mater. Process. Technol. 145 (1) (2004) 46–58.
[23] A. Parthiban, et al., Experimental investigation of turning parameters on AA 6061-T6 material, IOP Conf. Ser. Mater. Sci. Eng. 183 (2017), 012013.
[24] S. Bissey-Breton, J. Gravier, V. Vignal, Impact of superfinish turning on surface integrity of pure copper, Procedia Eng. 19 (2011) 28–33.
[25] Y. Li, et al., A study of aluminum bronze adhesion on tools during turning, J. Mater. Process. Technol. 138 (1) (2003) 479–483.
[26] V. Butenko, et al., Improving cutting wheels with a bakelite matrix, Russ. Eng. Res. 42 (5) (2022) 464–467.
[27] S. Prvulovic, et al., CHIP shape as machinability parameter in thermoplastic turning, Editura Politehnica 1 (2) (2018) 77, 2018.
[28] V. Pourmostaghimi, et al., A hybrid particle swarm optimization and recurrent dynamic neural network for multi-performance optimization of hard turning operation, AI EDAM (Artif. Intell. Eng. Des. Anal. Manuf.) 36 (2022) e28.
[29] S. Kim, K. Ahmadi, Estimation of vibration stability in turning using operational modal analysis, Mech. Syst. Signal Process. 130 (2019) 315–332.
[30] Y. Wang, et al., Structural coloration using face turning and variable tool vibration frequency, J. Manuf. Process56 (2020) 1392–1396.
[31] W. Chen, et al., Modelling and experimental investigation on textured surface generation in vibration-assisted micro-milling, J. Mater. Process. Technol. 266 (2019) 339–350.
[32] S.A. Sajjady, et al., Analytical and experimental study of topography of surface texture in ultrasonic vibration assisted turning, Mater. Des. 93 (2016) 311–323.
[33] H. Soleimanimehr, et al., The analysis of the Timoshenko transverse vibrations of workpiece in the ultrasonic vibration-assisted turning process and investigation of the machining error caused by this vibration, Precis. Eng. 54 (2018) 99–106.
[34] Z. Fu, et al., Modeling and investigation of the velocity-dependent cutting process with PDC cutters using the discrete element method, Shock Vib. (2023) 2023.
[35] J. Guo, et al., Regenerative effects of orthogonal chip dimensions on turning stability of thin-wall workpiece-tool coupled dynamics, IEEE ASME Trans. Mechatron. 27 (5) (2022) 3601–3612.
[36] R. Coppel, et al., Adaptive control optimization in micro-milling of hardened steels—evaluation of optimization approaches, Int. J. Adv. Des. Manuf. Technol. 84 (9) (2016) 2219–2238.
[37] Y. Koren, Adaptive control systems for machining, in: 1988 American Control Conference, 1988.
[38] V. Pourmostaghimi, et al., Application of evolutionary optimization techniques in reverse engineering of helical gears: an applied study, Axioms 12 (3) (2023) 252.

[39] V. Pourmostaghimi, M. Zadshakoyan, Designing and implementation of a novel online adaptive control with optimization technique in hard turning, Proc. IME J. Syst. Control Eng. 235 (5) (2020) 652–663.

[40] M. Moayyedian, M.R.C. Qazani, V. Pourmostaghim, Optimized injection-molding process for thin-walled polypropylene part using genetic programming and interior point solver, Int. J. Adv. Des. Manuf. Technol 124 (1–2) (2023) 297–313.

[41] M. Moayyedian, M.R.C. Qazani, V. Pourmostaghimi, Optimized injection-molding process for thin-walled polypropylene part using genetic programming and interior point solver, Int. J. Adv. Des. Manuf. Technol. 124 (1–2) (2023) 297–313.

[42] A. Seyyedabbasi, F. Kiani, Sand Cat swarm optimization: a nature-inspired algorithm to solve global optimization problems, Eng. Comput. (2022) 1–25.

[43] Z.-H. Zhou, Machine Learning, Springer Nature, 2021.

[44] M.I. Jordan, T.M. Mitchell, Machine learning: trends, perspectives, and prospects, Science 349 (6245) (2015) 255–260.

[45] E.H. Houssein, Machine learning and meta-heuristic algorithms for renewable energy: a systematic review, Advanced Control and Optimization Paradigms for Wind Energy Systems (2019) 165–187.

[46] J. Zhang, et al., Multi-objective optimization of concrete mixture proportions using machine learning and metaheuristic algorithms, Construct. Build. Mater. 253 (2020), 119208.

[47] L. Calvet, et al., Learnheuristics: hybridizing metaheuristics with machine learning for optimization with dynamic inputs, Open Math. 15 (1) (2017) 261–280.

[48] M. Karimi-Mamaghan, et al., Machine learning at the service of meta-heuristics for solving combinatorial optimization problems: a state-of-the-art, Eur. J. Oper. Res. 296 (2) (2022) 393–422.

[49] S.S. Nina Mazyavkina, Sergei ivanov, evgeny burnaev, Reinforcement Learning for Combinatorial Optimization: Surveyor 134 (2021), 105400.

[50] Q.W. Zhang, et al., Zigzag search for multi-objective optimization considering generation cost and emission, Appl. Energy 255 (2019), 113814.

[51] A.M. Zahir, et al., Objective functions modification of GA optimized PID controller for brushed DC motor, Int. J. Electr. Comput. Eng. 10 (3) (2020) 2426.

[52] P. Naeemi Amini, B. Moetakef-Imani, High-performance controller design and evaluation for active vibration control in boring, Sci. Iran. 26 (5) (2019) 2839–2853.

[53] S. Coromant, Tuning Guide, CoroKey, 2010, p. 120. English.